Journal of Materials Chemistry C

PAPER

View Article Online
View Journal | View Issue

Cite this: J. Mater. Chem. C, 2015, 3, 7567

Donor–acceptor–donor conjugated oligomers based on isoindigo and anthra[1,2-*b*]thieno[2,3-*d*]-thiophene for organic thin-film transistors: the effect of the alkyl side chain length on semiconducting properties†

Jing Shao,[ab] Xiaojie Zhang,[a] Hongkun Tian,*[a] Yanhou Geng*[a] and Fosong Wang[a]

Received 22nd May 2015,
Accepted 24th June 2015

DOI: 10.1039/c5tc01461a

www.rsc.org/MaterialsC

Three donor–acceptor–donor (D–A–D) conjugated oligomers, *i.e.*, **2ATT-IID-C8C10**, **2ATT-IID-C6C8** and **2ATT-IID-C4C6**, have been synthesized using anthra[1,2-*b*]thieno[2,3-*d*]thiophene (ATT) as an electron-donor unit and isoindigo (IID) as an electron-acceptor unit by combining the planar and rigid structure of fused aromatics and the strong intramolecular interaction of D–A conjugated molecules, and their semiconducting properties were studied *via* organic thin-film transistors (OTFTs). The alkyl chains, which are 2-octyldodecyl (C8C10), 2-hexyldecyl (C6C8) and 2-butyloctyl (C4C6), respectively, were employed in the IID unit in order to study the effect of alkyl bulkiness on the properties of the oligomers. All three oligomers adopted an edge-on alignment in thin films. Decreasing the bulkiness or length of the alkyls caused a noticeable improvement of the packing order of the oligomers, leading to a remarkably enhanced charge carrier mobility. **2ATT-IID-C8C10** could only form the film featured with one-dimensional order. Consequently, it exhibited the lowest OTFT mobility (<0.1 cm^2 V^{-1} s^{-1}). In contrast, both **2ATT-IID-C6C8** and **2ATT-IID-C4C6** adopted two-dimensional-ordered packing structures after thermal annealing with a π–π stacking distance of $\sim$3.6 Å, thereby exhibiting promising semiconducting properties. **2ATT-IID-C4C6** showed the best OTFT performance with a mobility of 0.72 cm^2 V^{-1} s^{-1}. This mobility is among the highest for the solution processible D–A conjugated oligomers to date.

1. Introduction

Organic semiconductors have been intensely investigated in recent years for their applications in printable electronics.[1–3] In the past several years, great progress has been achieved owing to the development of donor–acceptor (D–A) conjugated polymers, and a number of D–A conjugated polymers with a charge carrier mobility of >1 cm^2 V^{-1} s^{-1} have been reported.[4–37] Those with isoindigo (IID) derivatives as electron acceptor units particularly attracted interest for their remarkably high mobility,[31–40] and the mobility of organic thin-film transistors (OTFTs) based on these types of polymers has surpassed 10 cm^2 V^{-1} s^{-1}.[31] However, D–A conjugated polymers also have some disadvantages, such as strong aggregation in solution, broad distribution of molecular weight, low reproducibility in synthesis and difficult purification so on. These drawbacks may impede their future applications.

In contrast to conjugated polymers, conjugated oligomers are characterized by well-defined and uniform structures (*e.g.*, chain length, monomer sequence and chain ends) as well as high chemical purity accessible *via* recrystallization or column chromatography. Meanwhile, conjugated oligomers with moderate molecular weight are also solution processible. These features endow conjugated oligomers as promising materials for solution processed organic electronics. Although many D–A conjugated oligomers have been synthesized and characterized,[41–57] a few of them exhibited charge carrier mobility higher than 0.1 cm^2 V^{-1} s^{-1}.[53–57]

Introduction of polyaromatic units into the conjugated framework can enhance the intermolecular interaction due to their rigid and planar chemical structures, and is believed to be able to improve charge transport properties of organic semiconductors.[58] It is rational that D–A conjugated oligomers constructed with polyaromatics may have promising semiconducting properties. Thienoacenes are recently well-studied polyaromatics due to their high stability and synthetic accessibility.[59] Therefore, in the present paper, a series of donor–acceptor–donor (D–A–D)

[a] State key Laboratory of Polymer Physics and Chemistry, Changchun Institute of Applied Chemistry, Chinese Academy of Sciences, Changchun 130022, P. R. China. E-mail: yhgeng@ciac.ac.cn, hktian@ciac.ac.cn

[b] University of Chinese Academy of Sciences, Beijing 100049, P. R. China

† Electronic supplementary information (ESI) available: Other characterization data of the oligomers. See DOI: 10.1039/c5tc01461a

conjugated oligomers were synthesized by using anthra[1,2-*b*]-thieno[2,3-*d*]thiophene (ATT), a thienoacene comprising five fused rings, as an electron-donor unit and IID as an electron-acceptor unit and their semiconducting properties were investigated. Alkyl chains in the IID unit were also tuned in order to elaborate their influence on intermolecular packing structures and thereby charge transport properties of the oligomers.

2. Results and discussion

2.1. Synthesis and characterization

The synthesis of the oligomers is described in Scheme 1. Compound **1** was synthesized according to our previous report.[60] Stille couplings of **1** and IID derivatives **2a**, **2b** and **2c** with $Pd_2(dba)_3$/P(*o*-tolyl)$_3$ as a catalyst afforded **2ATT-IID-C8C10**, **2ATT-IID-C6C8** and **2ATT-IID-C4C6** in yields of 78, 84 and 86%, respectively. Although the solubility of the oligomers was decreased with a decrease of bulkiness of the alkyls in the IID unit, all three oligomers exhibited the solubility >6 mg mL^{-1} in chloroform, which is adequate for preparing thin films *via* spin-casting for characterization. Further cutting down the alkyl chain length resulted in a dramatic decrease of solubility. Chemical structures of **2ATT-IID-C8C10**, **2ATT-IID-C6C8** and **2ATT-IID-C4C6** were validated by NMR spectra, matrix-assisted laser desorption ionization time-of-flight (MALDI-TOF) mass spectra and elemental analysis. As shown in the mass spectra (see Fig. S1 in the ESI†), all oligomers showed one peak with the value consistent with their calculated molecular mass.

2.2. Thermal properties

Thermal properties of **2ATT-IID-C8C10**, **2ATT-IID-C6C8** and **2ATT-IID-C4C6** were studied by thermogravimetric analysis (TGA) and differential scanning calorimetry (DSC). All three oligomers are thermally stable with decomposition temperatures above 390 °C (5% weight loss, Fig. S2 in the ESI†). The DSC second heating scans of the oligomers are displayed in Fig. 1. As the alkyl chain length was reduced, the melting points of the oligomers were enhanced from 244 °C of **2ATT-IID-C8C10** to 261 °C of **2ATT-IID-C6C8** and then to 289 °C of **2ATT-IID-C4C6**. Besides, a weak transition was found at 154 °C for **2ATT-IID-C8C10**, which should be attributed to the transition between different crystalline states.

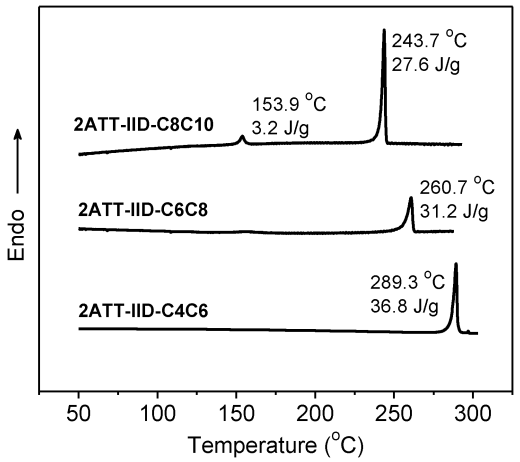

Fig. 1 DSC second heating scans of **2ATT-IID-C8C10**, **2ATT-IID-C6C8** and **2ATT-IID-C4C6** in nitrogen at a heating rate of 10 °C min^{-1}.

2.3. Optical and electrochemical properties

The solution and film absorption spectra of **2ATT-IID-C8C10**, **2ATT-IID-C6C8** and **2ATT-IID-C4C6** are shown in Fig. 2. In dilute solution, three oligomers exhibited identical absorption spectra (Fig. 2a), indicating a negligible effect of the alkyl chain on the photophysical properties of the oligomers in the ground state. Two featureless absorption bands were observed at 335 and 597 nm, which can be attributed to π–π* transition and intramolecular charge transfer (ICT) between the D and the A unit, respectively.[61,62] From solution to film, a red-shift less than 20 nm was observed for the π–π* transition absorption band. However, the long-wavelength absorption band exhibited a remarkable bathochromic shift along with the presence of three vibronic absorption peaks (Fig. 2b). These peaks are 562, 598 and 656 nm for **2ATT-IID-C8C10**, 560, 610, 663 nm for **2ATT-IID-C6C8** and 560, 612, 662 nm for **2ATT-IID-C4C6**. This indicates that the conjugated molecules re-organized in the film forming process and the planar conjugated backbones are strongly aggregated or closely packed in the solid state.[35,52] Moreover, the vibronic peak at 658–668 nm became stronger upon decreasing the bulkiness or the length of the alkyls in the IID unit, implying an enhanced aggregation tendency or intermolecular interaction from **2ATT-IID-C8C10** to **2ATT-IID-C6C8** and then to **2ATT-IID-C4C6**.[15] Obviously, the structure of alkyl chains has a great influence on the packing behaviour of current D–A conjugated oligomers in the solid state.

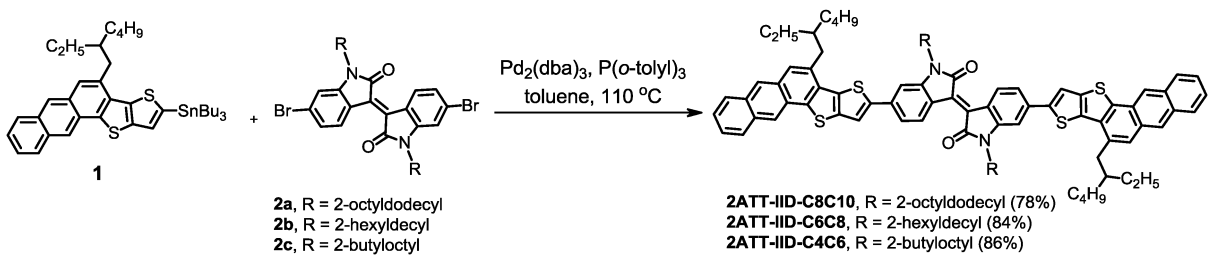

Scheme 1 Synthesis of D–A–D conjugated oligomers **2ATT-IID-C8C10**, **2ATT-IID-C6C8** and **2ATT-IID-C4C6**.

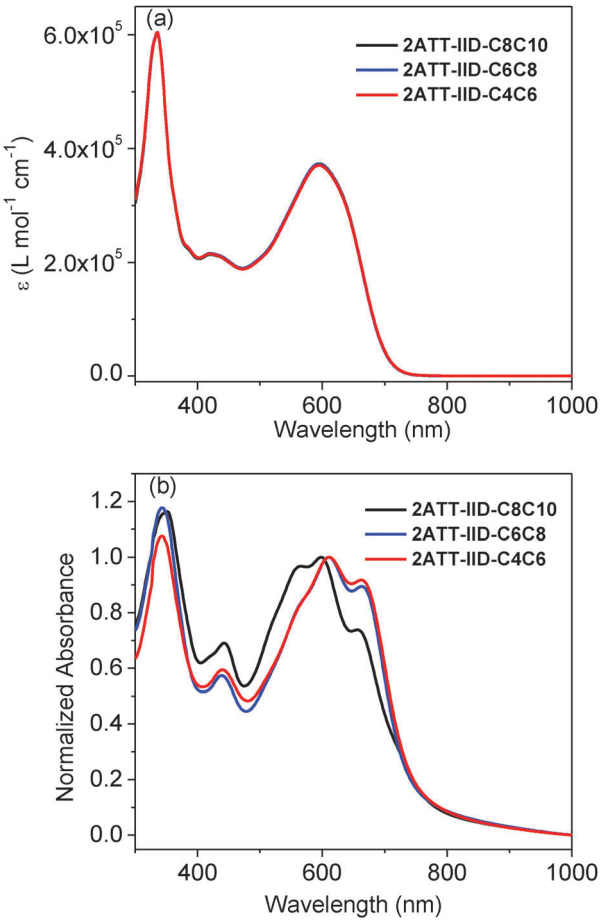

Fig. 2 Solution (a, 10^{-5} mol L^{-1} in $CHCl_3$) and film (b) UV-vis absorption spectra of **2ATT-IID-C8C10**, **2ATT-IID-C6C8** and **2ATT-IID-C4C6**. The films were prepared by spin-casting 6 mg mL^{-1} $CHCl_3$ solution on quartz substrates.

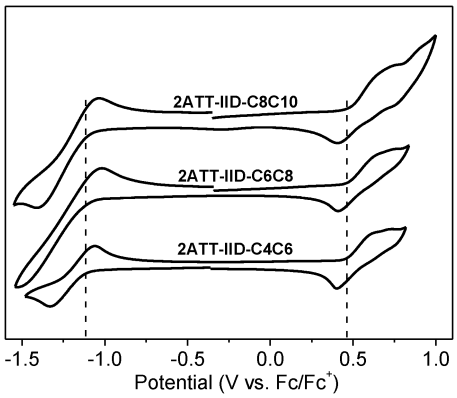

Fig. 3 Cyclic voltammograms (CV) of **2ATT-IID-C8C10**, **2ATT-IID-C6C8** and **2ATT-IID-C4C6** in chloroform (10^{-3} mol L^{-1}) with Bu_4NPF_6 (0.1 mol L^{-1}) as an electrolyte. The measurements were performed in a three-electrode cell with a Pt disk, a Pt wire and a calomel electrode as the working, counter and reference electrodes, respectively.

Cyclic voltammograms were measured to calculate the highest occupied molecular orbital (HOMO) and the lowest unoccupied molecular orbital (LUMO) energy levels. All three oligomers exhibited a reversible redox process in both positive and negative potential regions, their redox onset potentials are identical (Fig. 3 and Table 1). HOMO and LUMO energy levels are *ca.* −5.26 eV and −3.69 eV, respectively, as calculated from redox onsets according to the equations HOMO = $-(4.80 + E^{ox}_{onset})$ eV and LUMO = $-(4.80 + E^{re}_{onset})$.[63] Density functional theory (DFT) calculations were conducted to elucidate the properties of frontier molecular orbitals by replacing alkyl chains with methyl groups for simplifying the calculation. As shown in Fig. 4, similar to D–A conjugated polymers with IID as an A-unit,[7] the HOMO is delocalized over the entire molecule while the LUMO is centred on the IID unit.

2.4. Charge transport properties

To study their semiconducting properties, bottom-gate and top-contact OTFTs of **2ATT-IID-C8C10**, **2ATT-IID-C6C8** and **2ATT-IID-C4C6** were constructed on heavily doped n-type silicon wafers with 200 nm thermally grown SiO_2 (C_i = 17.3 nF cm^{-2}) *via* spin-casting with chloroform as a solvent. The substrates were pre-treated with octadecyltrichlorosilane (ODTS) following the reference procedure.[44] The thickness of the active layer is *ca.* 30 nm. All electric measurements of the devices were performed under ambient conditions and mobility (μ), threshold voltage (V_T) and the current on/off ratio (I_{on}/I_{off}) were calculated based on the standard metal-oxide-semiconductor field-effect transistor (MOSFET) equations in the saturation current regimes.[65] All three oligomers are typical p-type semiconductors. The devices based on pristine films exhibited maximum hole mobilities (μ_{max}s) of 5.1 × 10^{-3}, 0.11 and 0.081 cm^2 V^{-1} s^{-1} for **2ATT-IID-C8C10**, **2ATT-IID-C6C8** and **2ATT-IID-C4C6**, respectively (Table 2). Several thermal-annealing temperatures were selected for each oligomer to encourage the self-organization of the conjugated molecules and improve the device performance (Table S1, ESI†). The optimized thermal annealing temperatures were 100, 100 and 180 °C for **2ATT-IID-C8C10**, **2ATT-IID-C6C8** and **2ATT-IID-C4C6**, respectively. Fig. 5 shows the representative output and transfer curves of the devices based on thermally annealed films at optimized temperatures and the related data are summarized in Table 2. The output plots show well-defined linear and saturation regimes. After thermal annealing, the device performance was dramatically improved; and average mobility was improved from 4.2 × 10^{-3} cm^2 V^{-1} s^{-1} to 0.050 cm^2 V^{-1} s^{-1} for **2ATT-IID-C8C10**, 0.080 cm^2 V^{-1} s^{-1} to 0.23 cm^2 V^{-1} s^{-1} for **2ATT-IID-C6C8**, and 0.061 cm^2 V^{-1} s^{-1} to 0.61 cm^2 V^{-1} s^{-1} for **2ATT-IID-C4C6**. **2ATT-IID-C4C6** exhibited the highest mobility among three oligomers and its maximum mobility of 0.72 cm^2 V^{-1} s^{-1} is the highest among D–A conjugated oligomers reported so far.[55,56] These results indicate that high mobility conjugated oligomers are also accessible *via* rational molecular design.

2.5. Film morphology and microstructures

Fig. 6 reveals atomic force microscopic (AFM) images of the films of the oligomers. All films are uniform and featured with

Table 1 Optical and electrochemical properties of **2ATT-IID-C8C10**, **2ATT-IID-C6C8** and **2ATT-IID-C4C6**

	λ_{max} (nm)			
Oligomer	Solution[a]	Film	HOMO[b] (eV)/E^{ox}_{onset} (V)	LUMO[b] (eV)/E^{re}_{onset} (V)
2ATT-IID-C8C10	335, 597	350, 562, 598, 656	−5.27/0.47	−3.68/−1.12
2ATT-IID-C6C8	335, 597	343, 560, 610, 663	−5.26/0.46	−3.69/−1.11
2ATT-IID-C4C6	335, 597	342, 560, 612, 662	−5.26/0.46	−3.69/−1.11

[a] Measured in chloroform with a concentration of 10^{-5} mol L^{-1}. [b] The highest occupied molecular orbital (HOMO) and the lowest unoccupied molecular orbital (LUMO) energy levels were calculated according to HOMO = −(4.80 + E^{ox}_{onset}) eV and LUMO = −(4.80 + E^{re}_{onset}) eV, in which E^{ox}_{onset} and E^{re}_{onset} represent oxidation and reduction onset potentials, respectively.

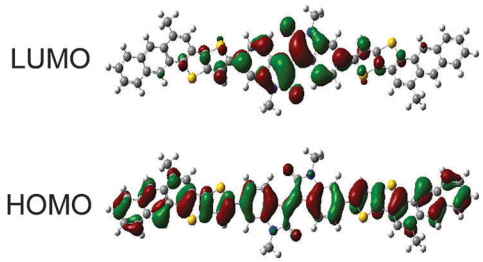

Fig. 4 DFT-optimized frontier molecular orbitals of **2ATT-IID** series (in B3LYP/6-31G level). Within calculation, all alkyl chains connected to the backbone are set as methyls.

Table 2 OTFT device performance of **2ATT-IID-C8C10**, **2ATT-IID-C6C8** and **2ATT-IID-C4C6**

Oligomer	T_a[a] (°C)	μ_{max}/μ_{ave}[b] ($cm^2\ V^{-1}\ s^{-1}$)	V_T[c] (V)	I_{on}/I_{off}[d]
2ATT-IID-C8C10	Pristine	0.0051/0.0042	−20 to −11	10^4–10^5
	100	0.082/0.050	−5 to 1	10^3–10^5
2ATT-IID-C6C8	Pristine	0.11/0.080	−10 to −2	10^4–10^8
	100	0.30/0.23	−15 to −9	10^4–10^7
2ATT-IID-C4C6	Pristine	0.081/0.061	−13 to −12	10^2–10^4
	180	0.72/0.61	−17 to −14	10^5–10^8

[a] Thermal annealing was carried out in nitrogen for 15 min. [b] Mobility calculated from the saturation regime, and average mobility was calculated from more than 5 parallel devices. [c] Threshold voltage. [d] Current on/off ratio.

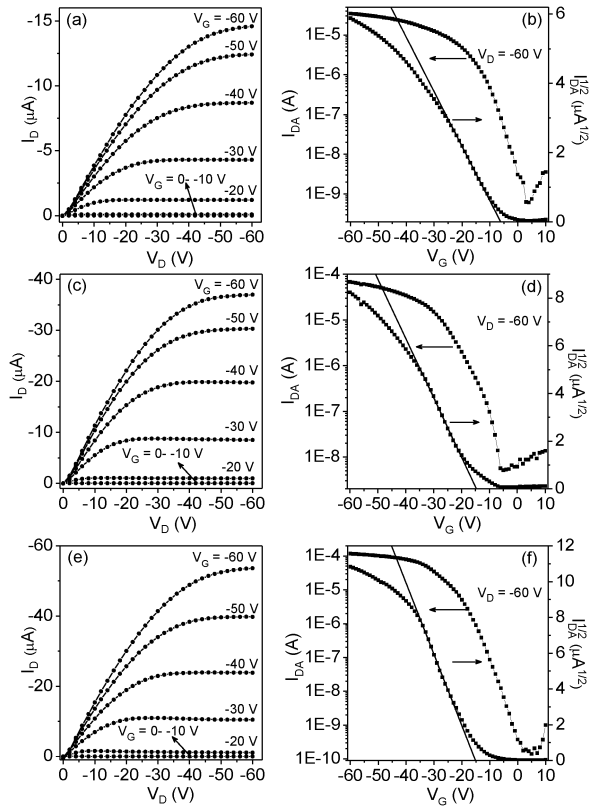

Fig. 5 Representative output (a, c and e) and transfer characteristics (b, d and f) of OTFT devices based on thermally annealed films of **2ATT-IID-C8C10** (a and b), **2ATT-IID-C6C8** (c and d) and **2ATT-IID-C4C6** (e and f). The annealing was done in nitrogen for 15 minutes at 100 °C for **2ATT-IID-C8C10** and **2ATT-IID-C6C8** and 180 °C for **2ATT-IID-C4C6**.

"granular" morphology. After thermal annealing, grain sizes and the surface roughness of the films were enlarged. Root mean square (RMS) values were increased from 1.92 nm to 2.92 nm for **2ATT-IID-C8C10**, 2.67 nm to 3.98 nm for **2ATT-IID-C6C8** and 1.89 nm to 4.12 nm for **2ATT-IID-C4C6**. This phenomenon is consistent with the improved device performance after thermal annealing, indicative of re-organization of conjugated molecules upon annealing.

To understand the insight of above results, two-dimensional grazing incidence X-ray diffraction (2D-GIXD) patterns of thin films (~30 nm) of the oligomers on Si/SiO_2 substrates were recorded to elucidate their packing structures in the solid state. As shown in Fig. 7, only the (100) diffraction peak at q_z = 0.34 $Å^{-1}$, corresponding to a *d*-spacing of 18.48 Å, was observed in the 2D-GIXD pattern of the pristine film of **2ATT-IID-C8C10**. The (100) diffraction peaks for the pristine films of **2ATT-IID-C6C8** (16.11 Å, q_z = 0.39 $Å^{-1}$) and **2ATT-IID-C4C6** (14.96 Å, q_z = 0.42 $Å^{-1}$) are much sharper and stronger than that of **2ATT-IID-C8C10** along with the presence of (200) diffractions. However, no diffraction peak originated from π–π stacking was observed along q_{xy} for the pristine films of all three oligomers. These results indicate that the oligomers packed in an edge-on way to form one-dimensional-ordered microstructures along the direction normal to the substrates, and the packing order of the conjugated skeletons was increased with a decrease of the bulkiness or length of alkyls in the IID unit. Thermal annealing resulted in a significant enhancement of the intermolecular packing order as evidenced by the enhanced diffraction intensity and the presence of diffraction peaks up to (200) for **2ATT-IID-C8C10** and diffraction peaks up to (300) for **2ATT-IID-C6C8** and **2ATT-IID-C4C6**. The *d*-spacings of (100) diffraction peaks are

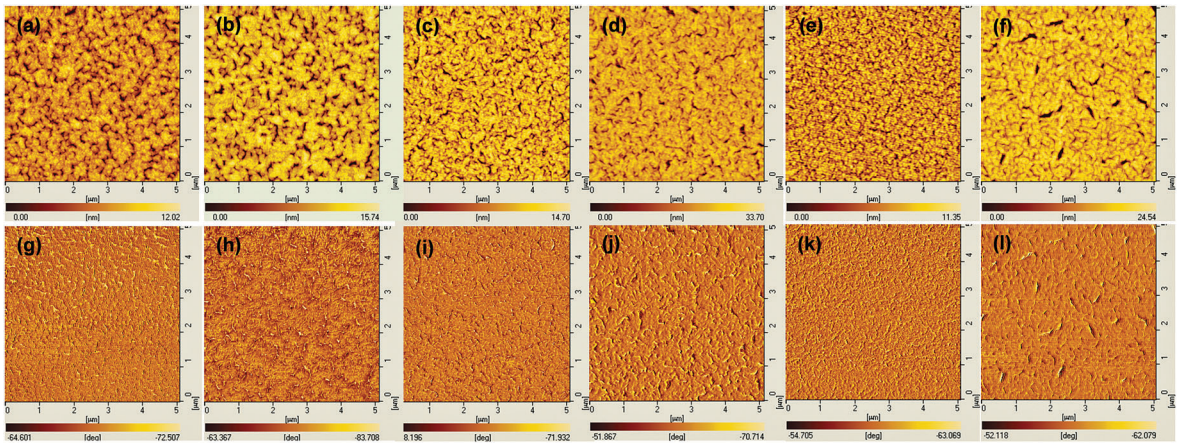

Fig. 6 Tapping mode AFM height (a–f) and phase (g–l) images of the films of **2ATT-IID-C8C10** (a, b, g and h), **2ATT-IID-C6C8** (c, d, i and j) and **2ATT-IID-C4C6** (e, f, k and l) before (a, c, e, g, i and k) and after thermal annealing (b, d, f, h, j and l). Thermal annealing was carried out at 100 °C for **2ATT-IID-C8C10** and **2ATT-IID-C6C8** and 180 °C for **2ATT-IID-C4C6**.

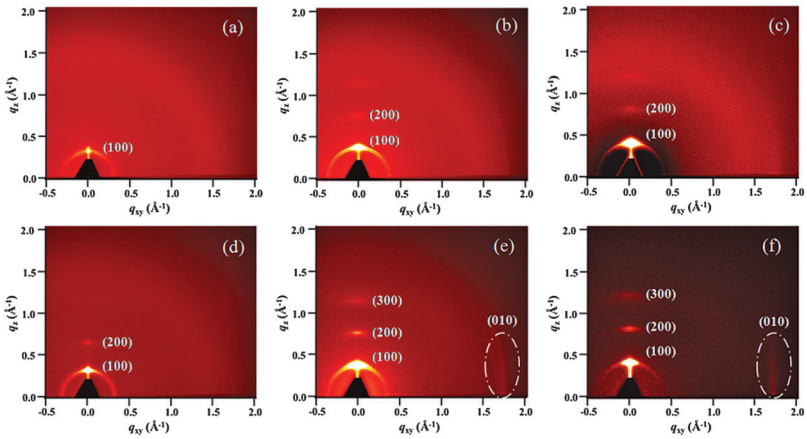

Fig. 7 2D-GIXD patterns of the films of **2ATT-IID-C8C10** (a and d), **2ATT-IID-C6C8** (b and e) and **2ATT-IID-C4C6** (c and f) before (a–c) and after (d and e) thermal annealing. Thermal annealing was carried out at 100 °C for **2ATT-IID-C8C10** and **2ATT-IID-C6C8** and 180 °C for **2ATT-IID-C4C6**.

18.73, 16.41 and 15.16 Å for **2ATT-IID-C8C10**, **2ATT-IID-C6C8** and **2ATT-IID-C4C6**, respectively. These values are slightly larger than those of pristine films. Most importantly, the thermally annealed films of **2ATT-IID-C6C8** and **2ATT-IID-C4C6** also exhibited the (010) diffraction peak along the q_{xy}-direction at q_{xy} = 1.74 Å^{-1} for **2ATT-IID-C6C8** and q_{xy} = 1.73 Å^{-1} for **2ATT-IID-C4C6**, corresponding to π–π stacking distances of 3.60 and 3.63 Å, respectively. These distance values are smaller than that of poly[2,2′-bithiophene-*alt*-*N*,*N*′-bis(2-octyldodecyl)isoindigo] (3.75 Å).[32,34] Note that the diffraction patterns became stronger and sharper from **2ATT-IID-C8C10** to **2ATT-IID-C6C8** and then to **2ATT-IID-C4C6** either for a pristine or a thermally annealed film. All the above results suggest that all three oligomers aligned in an edge-on feature in thin films, and the packing order was increased with a decrease of the bulkiness or the length of alkyls in the IID unit. **2ATT-IID-C8C10** adopted a one-dimensional packing structure even after thermal annealing, while **2ATT-IID-C6C8** and **2ATT-IID-C4C6** formed two-dimensional crystalline microstructures in the thin film after thermal annealing. These observations are consistent with the enhanced hole mobility from **2ATT-IID-C8C10** to **2ATT-IID-C6C8** and then to **2ATT-IID-C4C6.**

3. Conclusions

A series of D–A–D conjugated oligomers, *i.e.*, **2ATT-IID-C8C10**, **2ATT-IID-C6C8** and **2ATT-IID-C4C6**, have been designed and synthesized with fused aromatic ATT and IID as electron-donor and electron-acceptor units, respectively. The packing order of the conjugated skeletons in thin films was enhanced when the bulkiness or the length of the alkyls in the IID unit was decreased. **2ATT-IID-C8C10** only formed a one-dimensional-ordered packing structure, while **ATT-IID-C6C8** and **2ATT-IID-C4C6** could form two-dimensional-ordered packing structures after thermal annealing, leading to enhanced charge carrier transport properties from **2ATT-IID-C8C10** to **2ATT-IID-C6C8** and then to **2ATT-IID-C4C6**. The oligomer **2ATT-IID-C4C6** exhibited the best OTFT performance and a hole mobility of

0.72 $cm^2 V^{-1} s^{-1}$ has been realized. Our results suggest that high mobility conjugated oligomers can be prepared *via* rational molecular design.

4. Experimental section

4.1. Materials

Toluene was distilled after dried with sodium and benzophenone prior to use. The compounds tributyl(4-(2-ethylhexyl)anthra[1,2-*b*]thieno[2,3-*d*]thiophen-2-yl)stannane (**1**) and isoindigo derivatives **2** were prepared according to the reference procedure.[60,64] All other chemicals and solvents were used as received unless otherwise indicated.

4.2. Synthesis of oligomers

General procedure. Into a mixture of **1** (2.2 equiv.), IID derivatives (**2**, 1 equiv.), $Pd_2(dba)_3$ (4 mol%) and P(*o*-tolyl)$_3$ (32 mol%) anhydrous toluene was added under an Ar atmosphere with a concentration of 4×10^{-2} mol L^{-1} for **2**. The reaction mixture was stirred for 36 hours at 110 °C, cooled to room temperature, and then poured into saturated KF aqueous solution. The mixture was extracted with $CHCl_3$ and washed with brine. The organic extracts were separated and dried over $MgSO_4$. After the solvent was evaporated, the product was purified by column chromatography on the silica gel with $CHCl_3$/petroleum ether (1 : 2, v/v) as an eluent, and then recrystallized twice in toluene.

2ATT-IID-C8C10. Yield = 78%. δ_H (400 MHz, $CDCl_3$, Me_4Si) 9.13 (d, J = 8.4 Hz, 2H), 8.23 (s, 2H), 8.09 (s, 2H), 7.83 (d, J = 8.4 Hz, 2H), 7.71 (d, J = 8.4 Hz, 2H), 7.43 (s, 2H), 7.41 (s, 2H), 7.33 (m, 2H), 7.25 (m, 2H), 7.16 (d, J = 8.4 Hz, 2H), 6.80 (s, 2H), 3.76 (d, J = 6.8 Hz, 4H), 3.00 (m, 4H), 1.97 (m, 4H), 1.68–1.26 (m, 80H), 1.04–0.84 (m, 24H). δ_C (100 MHz, $CDCl_3$, Me_4Si) 168.46, 146.04, 145.32, 139.95, 137.98, 136.95, 135.20, 132.82, 131.50, 131.34, 131.07, 130.50, 130.28, 129.57, 127.83, 127.59, 126.81, 126.26, 125.50, 125.37, 124.96, 121.24, 120.44, 118.25, 116.00, 103.75, 44.55, 39.39, 38.43, 36.62, 31.97, 31.83, 30.23, 29.84, 29.76, 29.46, 28.44, 26.77, 25.25, 23.23, 22.75, 22.72, 14.25, 14.14, 10.50. Found. C, 79.51; H, 8.76; N, 1.50; S, 7.87%; M (MALDI-TOF-MS), 1622.9. $C_{108}H_{138}N_2O_2S_4$ requires C, 79.85; H, 8.56; N, 1.72; S, 7.90%; M, 1622.9.

2ATT-IID-C6C8. Yield = 84%. δ_H (400 MHz, $CDCl_3$, Me_4Si) 9.13 (d, J = 8.4 Hz, 2H), 8.23 (s, 2H), 8.09 (s, 2H), 7.82 (d, J = 8.4 Hz, 2H), 7.71 (d, J = 8.0 Hz, 2H), 7.43 (s, 2H), 7.41 (s, 2H), 7.33 (m, 2H), 7.25 (m, 2H), 7.16 (d, J = 8.4 Hz, 2H), 6.80 (s, 2H), 3.76 (d, J = 6.8 Hz, 4H), 3.00 (m, 4H), 1.97 (m, 4H), 1.67–1.26 (m, 64H), 1.04–0.82 (m, 24H). δ_C (100 MHz, $CDCl_3$, Me_4Si) 168.47, 146.05, 145.33, 139.95, 137.98, 136.97, 135.21, 132.82, 131.50, 131.35, 131.08, 130.49, 130.28, 129.56, 127.84, 127.59, 126.81, 126.27, 125.51, 125.38, 124.97, 121.24, 120.45, 118.27, 116.01, 103.77, 44.56, 39.40, 38.43, 36.61, 31.98, 31.83, 30.22, 29.86, 29.76, 29.46, 28.44, 26.77, 26.71, 25.24, 23.22, 22.76, 22.72, 14.26, 14.16, 14.14, 10.50. Found. C, 79.46; H, 8.31; N, 1.67; S, 8.31%; M (MALDI-TOF-MS), 1510.8. $C_{100}H_{122}N_2O_2S_4$ requires C, 79.42; H, 8.13; N, 1.85; S, 8.48%; M, 1510.8.

2ATT-IID-C4C6. Yield = 86%. δ_H (400 MHz, $CDCl_3$, Me_4Si) 9.10 (d, J = 8.4 Hz, 2H), 8.16 (s, 2H), 8.02 (s, 2H), 7.79 (d, J = 8.4 Hz, 2H), 7.65 (d, J = 8.4 Hz, 2H), 7.38 (s, 2H), 7.37 (s, 2H), 7.31–7.19 (m, 4H), 7.11 (d, J = 8.4 Hz, 2H), 6.75 (s, 2H), 3.75 (d, J = 6.8 Hz, 4H), 2.98 (m, 4H), 1.96 (m, 4H), 1.53–1.26 (m, 48H), 1.03–0.88 (m, 24H). The solubility is not adequate for ^{13}C NMR. Found. C, 78.71; H, 7.98; N, 1.87; S, 9.03%; M (MALDI-TOF-MS), 1398.7. $C_{92}H_{106}N_2O_2S_4$ requires C, 78.92; H, 7.63; N, 2.00; S, 9.16%; M, 1398.7.

4.3. Instruments and methods

^1H NMR and ^{13}C NMR spectra were recorded on a Bruker 400 MHz spectrometer in $CDCl_3$ with tetramethylsilane (TMS) as internal reference. MALDI-TOF mass spectra were measured using a Bruker/AutoflexIII Smartbean MALDI mass spectrometer with 2-[(2*E*)-3-(4-*tert*-butylphenyl)-2-methylprop-2-enylidene]-malononitrile (DCTB) as a substrate. Elemental analysis was carried out using a VarioEL elemental analysis system. TGA was performed on a Perkin-Elmer TGA-7 at a heating rate of 10 °C min^{-1} under nitrogen flow of 20 mL min^{-1}. DSC was conducted on a Perkin-Elmer DSC7 thermal analyzer at a heating/cooling rate of 10/−10 °C min^{-1} under nitrogen flow of 20 mL min^{-1}. UV-vis absorption spectra were measured on a Perkin-Elmer Lambda 35 spectrometer. CV measurements were carried out on a CHI660a electrochemical analyzer in anhydrous chloroform with Bu_4NPF_6 as an electrolyte at a scan rate of 100 mV s^{-1}. A three-electrode system was used with a Pt disk (2 mm diameter) electrode, a saturated calomel electrode and a Pt wire as the working, reference and counter electrodes, respectively. The potential was calibrated against the ferrocene/ferrocenium couple. AFM images were measured on a SPI3800N (Seiko Instruments Inc., Japan) in the tapping mode. The two dimensional grazing incidence X-ray diffraction (GIXD) was measured at Shanghai Synchrotron Radiation Facility (SSRF) on beam line BL14B1 (λ = 0.124 nm) using a MarCCD area detector at an incidence angle of 0.16°.

4.4. OTFT fabrication and measurement

n-Doped Si wafers with 200 nm thickness of SiO_2 were used as the gate electrode and dielectric layer. The substrates were pre-treated with ODTS following the reference procedure.[44] Thin films were deposited by spin-casting 0.4% (w/w) $CHCl_3$ solutions of the oligomers at 2000 rpm. Thermal annealing was done in a glove box (15 min). Au drain and source electrodes (thickness 40 nm) were deposited in a vacuum through a shadow mask. The channel length (L) and width (W) are 100 μm and 3000 μm, respectively. The electrical measurements were performed using two Keithley 236 source/measure units at room temperature in an ambient atmosphere.

Acknowledgements

This work is supported by National Basic Research Program of China (973 Project, No. 2014CB643504) of Chinese Ministry of Science and Technology, the National Natural Science Foundation of China (No. 51333006) and the Strategic Priority Research

Program of the Chinese Academy of Sciences (No. XDB12010300). The authors also thank the Shanghai Synchrotron Radiation Facility (SSRF) for the help with 2D-GIXD measurements.

Notes and references

1 C. Wang, H. Dong, W. Hu, Y. Liu and D. Zhu, *Chem. Rev.*, 2012, **112**, 2208.
2 J. Mei, Y. Diao, A. L. Appleton, L. Fang and Z. Bao, *J. Am. Chem. Soc.*, 2013, **135**, 6724.
3 H. Sirringhaus, *Adv. Mater.*, 2014, **26**, 1319.
4 W. Zhang, J. Smith, S. E. Watkins, R. Gysel, M. McGehee, A. Salleo, J. Kirkpatrick, S. Ashraf, T. Anthopoulos, M. Heeney and I. McCulloch, *J. Am. Chem. Soc.*, 2010, **132**, 11437.
5 H. Bronstein, Z. Chen, R. S. Ashraf, W. Zhang, J. Du, J. R. Durrant, P. S. Tuladhar, K. Song, S. E. Watkins, Y. Geerts, M. M. Wienk, R. A. J. Janssen, T. Anthopoulos, H. Sirringhaus, M. Heeney and I. McCulloch, *J. Am. Chem. Soc.*, 2011, **133**, 3272.
6 H. N. Tsao, D. M. Cho, I. Park, M. R. Hansen, A. Mavrinskiy, D. Y. Yoon, R. Graf, W. Pisula, H. W. Spiess and K. Müllen, *J. Am. Chem. Soc.*, 2011, **133**, 2605.
7 J. D. Yuen, J. Fan, J. Seifter, B. Lim, R. Hufschmid, A. J. Heeger and F. Wudl, *J. Am. Chem. Soc.*, 2011, **133**, 20799.
8 J. S. Ha, K. H. Kim and D. H. Choi, *J. Am. Chem. Soc.*, 2011, **133**, 10364.
9 Y. Li, P. Sonar, S. P. Singh, W. Zeng and M. S. Soh, *J. Mater. Chem.*, 2011, **21**, 10829.
10 Z. Chen, M. J. Lee, R. S. Ashraf, Y. Gu, S. Albert-Seifried, M. M. Nielsen, B. Schroeder, T. D. Anthopoulos, M. Heeney, I. McCulloch and H. Sirringhaus, *Adv. Mater.*, 2012, **24**, 647.
11 J. S. Lee, S. K. Son, S. Song, H. Kim, D. R. Lee, K. Kim, M. J. Ko, D. H. Choi, B. Kim and J. H. Cho, *Chem. Mater.*, 2012, **24**, 1316.
12 J. Fan, J. D. Yuen, W. Cui, J. Seifter, A. R. Mohebbi, M. Wang, H. Zhou, A. Heeger and F. Wudl, *Adv. Mater.*, 2012, **24**, 6164.
13 Y. Deng, Y. Chen, X. Zhang, H. Tian, C. Bao, D. Yan, Y. Geng and F. Wang, *Macromolecules*, 2012, **45**, 8621.
14 J. Lee, A.-R. Han, J. Kim, Y. Kim, J. H. Oh and C. Yang, *J. Am. Chem. Soc.*, 2012, **134**, 20713.
15 H. Chen, Y. Guo, G. Yu, Y. Zhao, J. Zhang, D. Gao, H. Liu and Y. Liu, *Adv. Mater.*, 2012, **24**, 4618.
16 M. Shahid, T. McCarthy-Ward, J. Labram, S. Rossbauer, E. B. Domingo, S. E. Watkins, N. Stingelin, T. D. Anthopoulos and M. Heeney, *Chem. Sci.*, 2012, **3**, 181.
17 J. Fan, J. D. Yuen, M. Wang, J. Seifter, J.-H. Seo, A. R. Mohebbi, D. Zakhidov, A. Heeger and F. Wudl, *Adv. Mater.*, 2012, **24**, 2186.
18 H.-W. Lin, W.-Y. Lee and W.-C. Chen, *J. Mater. Chem.*, 2012, **22**, 2120.
19 X. Zhang, H. Bronstein, A. J. Kronemeijer, J. Smith, Y. Kim, R. J. Kline, L. J. Richter, T. D. Anthopoulos, H. Sirringhaus, K. Song, M. Heeney, W. Zhang, I. McCulloch and D. M. DeLongchamp, *Nat. Commun.*, 2013, **4**, 2238.
20 J. Lee, A.-R. Han, H. Yu, T. J. Shin, C. Yang and J. H. Oh, *J. Am. Chem. Soc.*, 2013, **135**, 9540.
21 Q. Wu, M. Wang, X. Qiao, Y. Xiong, Y. Huang, X. Gao and H. Li, *Macromolecules*, 2013, **46**, 3887.
22 J. R. Matthews, W. Niu, A. Tandia, A. L. Wallace, J. Hu, W.-Y. Lee, G. Giri, S. C. B. Mannsfeld, Y. Xie, S. Cai, H. H. Fong, Z. Bao and M. He, *Chem. Mater.*, 2013, **25**, 782.
23 M. J. Cho, J. Shin, S. H. Yoon, T. W. Lee, M. Kaur and D. H. Choi, *Chem. Commun.*, 2013, **49**, 7132.
24 C. Cheng, C. Yu, Y. Guo, H. Chen, Y. Fang, G. Yu and Y. Liu, *Chem. Commun.*, 2013, **49**, 1998.
25 Z. Yi, L. Ma, B. Chen, D. Chen, X. Chen, J. Qin, X. Zhan, Y. Liu, W. J. Ong and J. Li, *Chem. Mater.*, 2013, **25**, 4290.
26 Z. Chen, P. Cai, J. Chen, X. Liu, L. Zhang, L. Lan, J. Peng, Y. Ma and Y. Cao, *Adv. Mater.*, 2014, **26**, 2586.
27 B. Fu, J. Baltazar, A. R. Sankar, P.-H. Chu, S. Zhang, D. M. Collard and E. Reichmanis, *Adv. Funct. Mater.*, 2014, **24**, 3734.
28 H.-R. Tseng, H. Phan, C. Luo, M. Wang, L. A. Perez, S. N. Patel, L. Ying, E. J. Kramer, T.-Q. Nguyen, G. C. Bazan and A. J. Heeger, *Adv. Mater.*, 2014, **26**, 2993.
29 I. Kang, H.-J. Yun, D. S. Chung, S.-K. Kwon and Y.-H. Kim, *J. Am. Chem. Soc.*, 2013, **135**, 14896.
30 J. Li, Y. Zhao, H. S. Tan, Y. Guo, C.-A. Di, G. Yu, Y. Liu, M. Lin, S. H. Lim, Y. Zhou, H. Su and B. S. Ong, *Sci. Rep.*, 2012, **2**, 754.
31 G. Kim, S.-J. Kang, G. K. Dutta, Y.-K. Han, T. J. Shin, Y.-Y. Noh and C. Yang, *J. Am. Chem. Soc.*, 2014, **136**, 9477.
32 J. Mei, D. H. Kim, A. L. Ayzner, M. F. Toney and Z. Bao, *J. Am. Chem. Soc.*, 2011, **133**, 20130.
33 T. Lei, J.-H. Dou, Z.-J. Ma, C.-H. Yao, C.-J. Liu, J.-Y. Wang and J. Pei, *J. Am. Chem. Soc.*, 2012, **134**, 20025.
34 T. Lei, J.-H. Dou and J. Pei, *Adv. Mater.*, 2012, **24**, 6457.
35 T. Lei, Y. Cao, X. Zhou, Y. Peng, J. Bian and J. Pei, *Chem. Mater.*, 2012, **24**, 1762.
36 T. Lei, J.-H. Dou, Z.-J. Ma, C.-J. Liu, J.-Y. Wang and J. Pei, *Chem. Sci.*, 2013, **4**, 2447.
37 J. Shin, H. A. Um, D. H. Lee, T. W. Lee, M. J. Cho and D. H. Choi, *Polym. Chem.*, 2013, **4**, 5688.
38 R. Stalder, J. Mei, K. R. Graham, L. A. Estrada and J. R. Reynolds, *Chem. Mater.*, 2014, **26**, 664.
39 T. Lei, J.-Y. Wang and J. Pei, *Acc. Chem. Res.*, 2014, **47**, 1117.
40 P. Deng and Q. Zhang, *Polym. Chem.*, 2014, **5**, 3298.
41 S. Loser, C. J. Bruns, H. Miyauchi, R. P. Ortiz, A. Facchetti, S. I. Stupp and T. J. Marks, *J. Am. Chem. Soc.*, 2011, **133**, 8142.
42 S. Loser, H. Miyauchi, J. W. Hennek, J. Smith, C. Huang, A. Facchetti and T. J. Marks, *Chem. Commun.*, 2012, **48**, 8511.
43 W. W. H. Wong, J. Subbiah, S. R. Puniredd, B. Purushothaman, W. Pisula, N. Kirby, K. Müllen, D. J. Jones and A. B. Holmes, *J. Mater. Chem.*, 2012, **22**, 21131.
44 Y. Zhang, C. Kim, J. Lin and T.-Q. Nguyen, *Adv. Funct. Mater.*, 2012, **22**, 97.
45 J. Liu, Y. Sun, P. Moonsin, M. Kuik, C. M. Proctor, J. Lin, B. B. Hsu, V. Promarak, A. J. Heeger and T.-Q. Nguyen, *Adv. Mater.*, 2013, **25**, 5898.

46 J. Liu, B. Walker, A. Tamayo, Y. Zhang and T.-Q. Nguyen, *Adv. Funct. Mater.*, 2013, **23**, 47.
47 L. Wang, X. Zhang, H. Tian, Y. Lu, Y. Geng and F. Wang, *Chem. Commun.*, 2013, **49**, 11272.
48 S.-Y. Liu, W.-Q. Liu, J.-Q. Xu, C.-C. Fan, W.-F. Fu, J. Ling, J.-Y. Wu, M.-M. Shi, A. K.-Y. Jen and H.-Z. Chen, *ACS Appl. Mater. Interfaces*, 2014, **6**, 6765.
49 S.-Y. Liu, W.-F. Fu, J.-Q. Xu, C.-C. Fan, H. Jiang, M. Shi, H.-Y. Li, J.-W. Chen, Y. Cao and H.-Z. Chen, *Nanotechnology*, 2014, **25**, 014006.
50 P. Sonar, E. L. Williams, S. P. Singh, S. Manzhos and A. Dodabalapur, *Phys. Chem. Chem. Phys.*, 2013, **15**, 17064.
51 A. K. Palai, J. Lee, M. Jea, H. Na, T. J. Shin, S. Jang, S.-U. Park and S. Pyo, *J. Mater. Sci.*, 2014, **49**, 4215.
52 W. Elsawy, C.-L. Lee, S. Cho, S.-H. Oh, S.-H. Moon, A. Elbarbary and J.-S. Lee, *Phys. Chem. Chem. Phys.*, 2013, **15**, 15193.
53 C. Lu and W. Chen, *Chem. – Asian J.*, 2013, **8**, 2813.
54 A. Riaño, P. M. Burrezo, M. J. Mancheño, A. Timalsina, J. Smith, A. Facchetti, T. J. Marks, J. T. L. Navarrete, J. L. Segura, J. Casado and R. P. Ortiz, *J. Mater. Chem. C*, 2014, **2**, 6376.
55 C. Yu, Z. Liu, Y. Yang, J. Yao, Z. Cai, H. Luo, G. Zhang and D. Zhang, *J. Mater. Chem. C*, 2014, **2**, 10101.
56 S. S. Dharmapurikar, A. Arulkashmir, C. Das, P. Muddellu and K. Krishnamoorthy, *ACS Appl. Mater. Interfaces*, 2013, **5**, 7086.
57 A. K. K. Kyaw, D. H. Wang, V. Gupta, W. L. Leong, L. Ke, G. C. Bazan and A. J. Heeger, *ACS Nano*, 2013, **7**, 4569.
58 V. Coropceanu, J. Cornil, D. A. da Silva Filho, Y. Olivier, R. Silbey and J.-L. Brédas, *Chem. Rev.*, 2007, **107**, 926.
59 K. Takimiya, S. Shinamura, I. Osaka and E. Miyazaki, *Adv. Mater.*, 2011, **23**, 4347.
60 J. Shao, X. Zhao, L. Wang, Q. Tang, W. Li, H. Yu, H. Tian, X. Zhang, Y. Geng and F. Wang, *Tetrahedron Lett.*, 2014, **55**, 5663.
61 E. Bundgaard and F. C. Krebs, *Sol. Energy Mater. Sol. Cells*, 2007, **91**, 954.
62 G. Brocks and A. Tol, *J. Phys. Chem.*, 1996, **100**, 1838.
63 C. M. Cardona, W. Li, A. E. Kaifer, D. Stockdale and G. C. Bazan, *Adv. Mater.*, 2011, **24**, 2367.
64 J. Mei, K. R. Graham, R. Stalder and J. R. Reynolds, *Org. Lett.*, 2010, **12**, 660.
65 C. D. Dimitrakopoulos and P. R. L. Malenfant, *Adv. Mater.*, 2002, **14**, 99.

